Supplementary Information

Ternary NiFeZr layered double hydroxides nanosheets: an highly efficient catalyst for oxygen evolution reaction

1. Experimental Section

Chemicals:

Nickel (II) nitrate hexahydrate (Ni $(NO_3)_2 \cdot 6H_2O$, 98%, Kermel), iron (III) nitrate nonahydrate (Fe $(NO_3)_3 \cdot 9H_2O$, Aladdin), zirconium (IV) oxychloride octahydrate ($ZrOCl_2 \cdot 8H_2O$, 99%, Kermel), urea ($CO(NH_2)_2$, 99%, AR, Kermel), Potassium hydroxide (KOH, 98%, Kermel), hydrochloric acid (HCl, 36-38 wt%, Xilong Scientific), iridium oxide powder (IrO_2, 99%, Aladdin), Nickel foam, deionized water. Deionized water was used for the preparation of all aqueous solutions. All reagents used in the experiments were of analytical grade, and no further processing was required.

Pretreatment of Ni foam:

In a reformative procedure, the nickel foam (about 3*4 cm^2) was first cleaned with 40 ml of deionized water and 10 ml of 1M HCl solution by ultrasonic treatment for 10 min. The nickel oxide layer on the surface of the nickel foam was removed by reaction with H^+ in the solution. Subsequently, the nickel foam was sonicated for 10 minutes in deionized water and ethanol respectively to ensure that the nickel foam was clean, and then drying naturally at 60 °C.

Fabrication of NiFeZr LDHs:

Ni $(NO_3)_2 \cdot 6H_2O$ (1.8 mmol), $ZrOCl_2 \cdot 8H_2O$ (0.45 mmol), Fe $(NO_3)_3 \cdot 9H_2O$ (0.45 mmol), and urea (4.5 mmol) were dissolved in 60 mL of deionized water, sonicated for about 15 min to form a clear and transparent solution. Put the above solution together with clean foam nickel into a 100 ml Teflon-lined stainless-steel autoclave, and then keep the reaction at 120 °C for 12 h. After the reaction, the NiFeZr LDHs were naturally cooled to room temperature, and the final products were ultrasonic for 5 min in a of ethanol-deionized water mixture with a volume ratio of 1:1, then rinsed several repeats with deionized water and ethanol respectively respectively, and subsequently dried at 60 °C for 10 h. The weight of catalyst is about 4 mg cm^{-2} on the

surface of the nickel foam. In addition, NiFeZr LDHs with different initial metal salt ratios were prepared, in which the molar ratios of Ni $(NO_3)_2 \cdot 6H_2O$, Fe $(NO_3)_3 \cdot 9H_2O$ and $ZrOCl_2 \cdot 8H_2O$ were 4:0.5:1.5, 4:1.5:0.5, 3:1:1, 5:1:1, 6:1:1, respectively.

Fabrication of NiFe LDHs, NiZr LDHs and Ni $(OH)_2$:

NiFe LDHs and NiZr LDHs nanosheets were prepared by the above method. The difference was that the initial metal salts of NiFe LDHs were Ni $(NO_3)_2 \cdot 6H_2O$ (1.8 mmol) and Fe $(NO_3)_3 \cdot 9H_2O$ (0.9 mmol), while the initial metal salts of NiZr LDHs were Ni $(NO_3)_2 \cdot 6H_2O$ (1.8 mmol) and $ZrOCl_2 \cdot 8H_2O$ (0.9 mmol). The Ni $(OH)_2$ nanoarrays was synthesized by the above method only with Ni $(NO_3)_2 \cdot 6H_2O$ (2.7 mmol) and urea (4.5 mmol).

Fabrication of IrO_2/C electrode on Ni foam:

To acquire the 40wt% IrO_2/C electrode, 4 mg IrO_2 powder, 6 mg carbon black (Vulcan XC-72R), and 60 μL nafion were mixed with 1 mL N, N-dimethyl formamide by ultrasonication for about 15 min. Next, 40% of the obtained homogeneous ink was coated onto a bare Ni foam substrate with a geometric area of 1 cm^2, which appointed as IrO_2/C for comparison.

Electrochemical Measurements:

The electrochemical measurements were carried out at room temperature in a three-electrode glass cell connected to an electrochemical workstation (CHI 760A, CH, Shanghai.). The potentials vs Hg/HgO recorded in alkaline media were displayed versus RHE by the following Nernst equation without otherwise noted:

$$E(RHE) = E(Hg/HgO) + 0.098 + 0.059 \times pH \quad \text{(eq 1)}$$

Then, the gained potentials were corrected for iR drop by another equation:

$$E(iR) = E(RHE) - iR \quad \text{(eq 2)}$$

where E(iR) denotes the actual applied bias vs. RHE and iR represents the voltage drop caused by the solution. And, the overpotential (η) is the potential difference between E(RHE) and the theoretical minimum potential (1.23 V) required for electrolyzed water. The current density (J) indicated was was calculated according to the geometric area of the electrode. Meanwhile, Tafel slopes were obtained based on the Tafel Equation:

$$E(iR) = b*\log(/ J /) + a \quad \text{(eq 3)}$$

where b and J respectively denote the Tafel slope and the current density. The double-layer capacitor (C_{dl}) is measured by CV at a scan rate of 10, 20, 30, 40, 50 mV s^{-1} without Faraday current, and current density average differences(ΔJ) is obtained

through dividing the CV integral area by the potential difference (0.1 V). The ECSA is the ratio of the Cdl of the electrode to the specific capacitance (C_s) of the ideal smooth electrode with a geometric area of 1 cm^2, see the equation 4:

$$ECSA = A^* C_{dl} / C_s \quad \text{(eq 4)}$$

where A is the geometric area, and the value of C_s ranges from 20-60 mF cm^{-2}, where C_s = 40 mF cm^{-2} is used to calculate the ECSA of samples.[1] And normalized current densities(J_{ECSA}) were acquired through dividing by the ECSAs.

Characterizations of materials:

The crystalline structure of the sample was analyzed by X-ray diffraction (XRD, D/MAX-2500) with a Cu-K α radiation source. Scanning electron microscope (SEM, S-4800) was applied to investigate the morphology and corresponding energy dispersion X-ray mapping of the samples. And transmission electron microscope (TEM, Talos F200X) was used for the microstructure analysis of the samples. The chemical states of element were determined by X-ray photoelectron spectroscopy (XPS) using a Per-kin-Elmer PHI5300ESCALAB 250Xi with Al Kα as the X ray source.

2. Figures

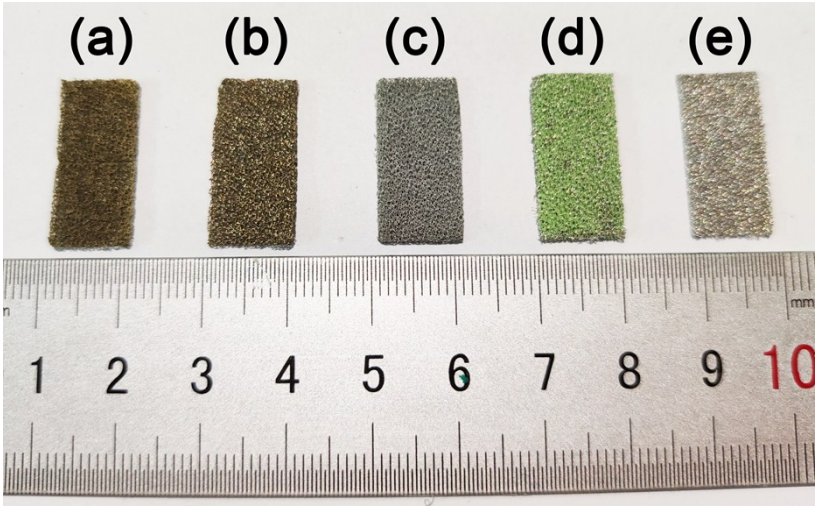

Fig. S1 Optical images of (a) NiFeZr LDHs nanosheets, (b) NiFe LDHs nanosheets, (c) NiZr LDHs nanosheets, (d) Ni $(OH)_2$ on Ni foam, (e) pure nickel foam. The color of as-prepared NiFeZr LDHs nanosheets is different from those of samples.

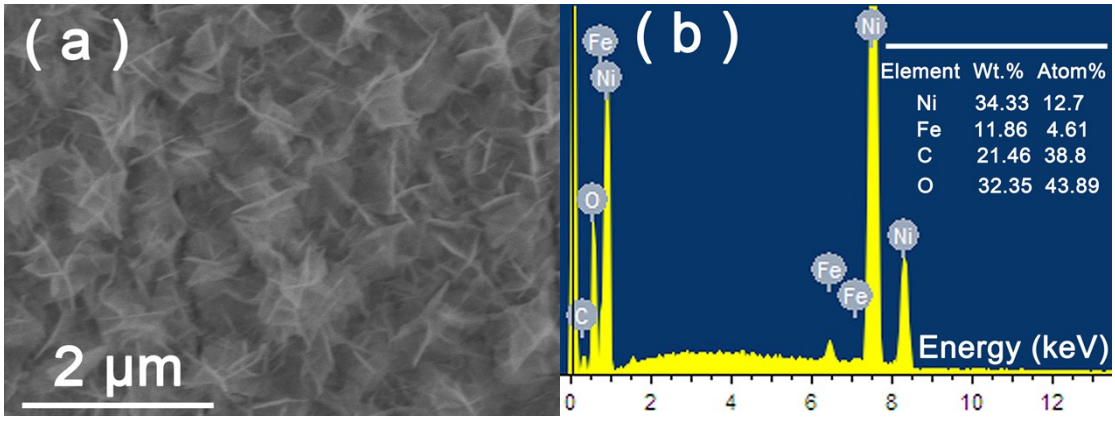

Fig. S2 (a) SEM image of NiFe LDHs nanosheets. (b) EDS spectra and corresponding elements ratio of NiFe LDHs nanosheets.

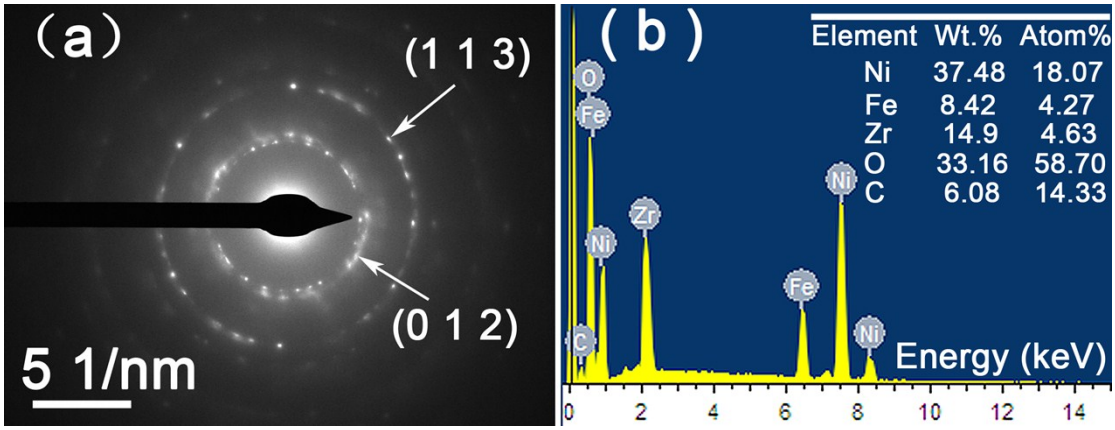

Fig. S3 (a) SAED patterns of NiFeZr LDHs, demonstrating the crystal structure of NiFeZr LDHs nanosheets. (b) EDS spectra and corresponding element ratio of NiFeZr LDHs.

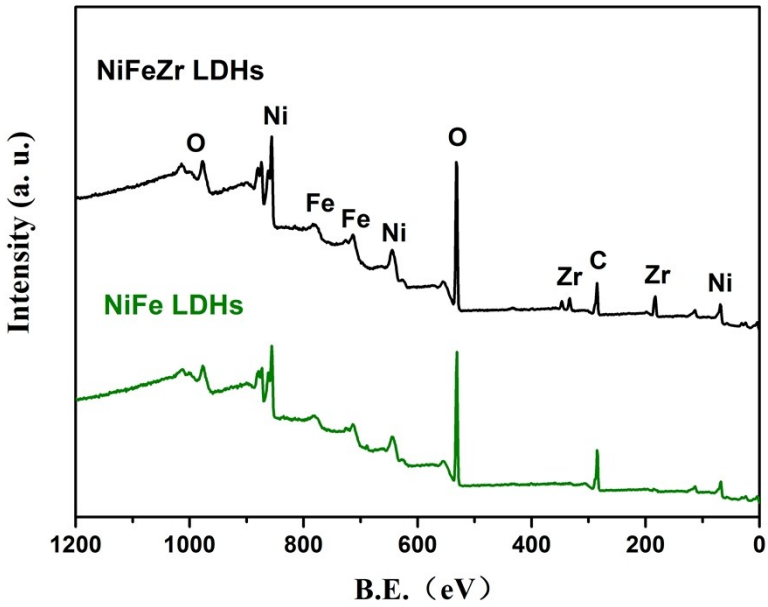

Fig. S4 The XPS profile survey spectra for both NiFeZr LDHs and NiFe LDHs.

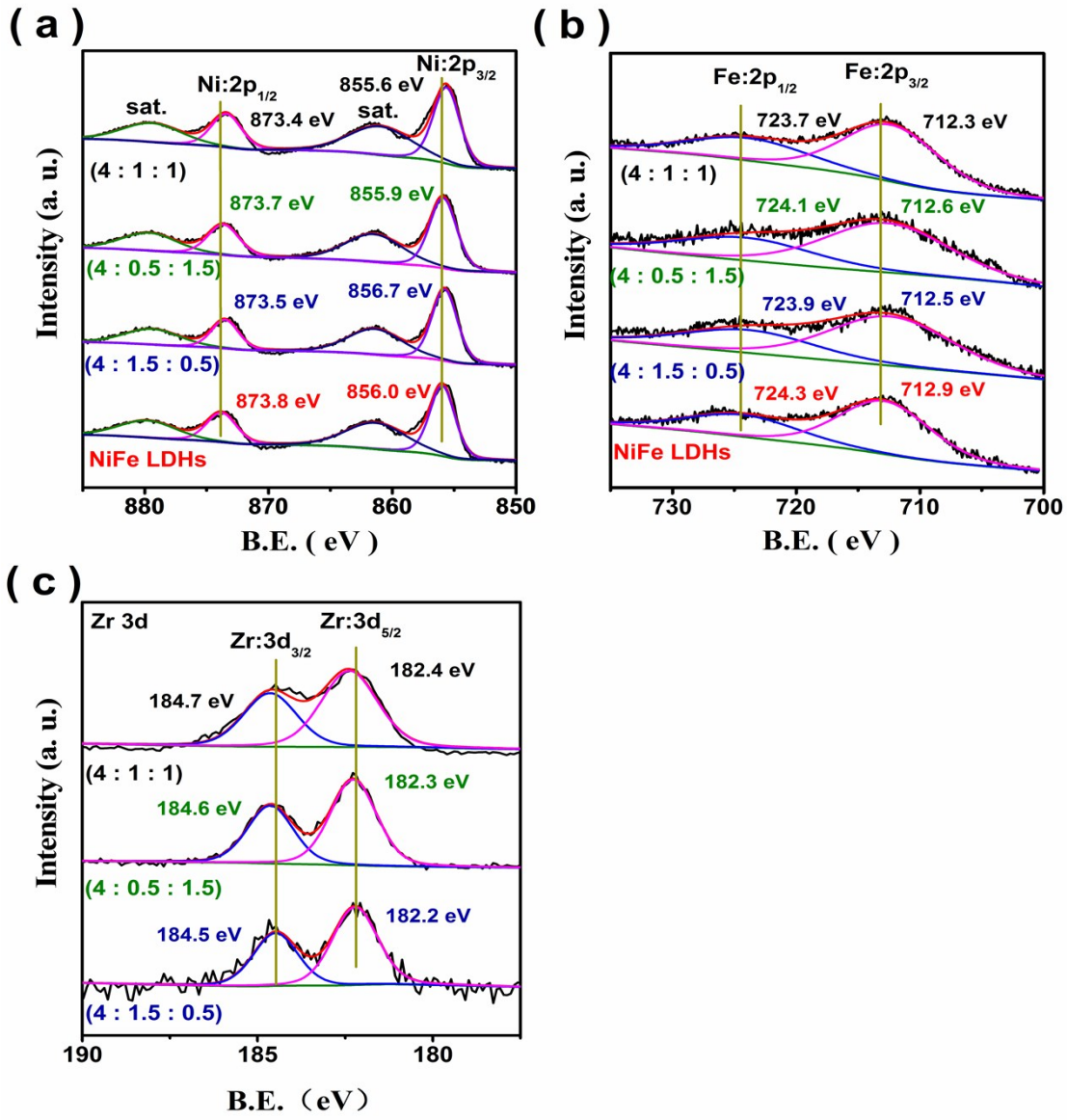

Fig. S5 High resolution XPS spectrums of (a) Ni 2p, (b) Fe 2p, (c) Zr 3d for NiFeZr LDHs (d) Zr 3d for the NiFeZr LDHs with different starting material feed ratios of metal salts. The (4:1:1), (4:0.5:1.5), and (4:1.5:0.5) were respectively NiFeZr LDHs (4:1:1), NiFeZr LDHs (4:0.5:1.5), and NiFeZr LDHs (4:1.5:0.5). Obviously, when the Fe:Zr ratio was 1:1, the characteristic peaks of Ni 2p and Fe 2p were shifted to lower binding energy, and the characteristic peaks of Zr 3d were shifted to higher binding energy, compared with other Fe:Zr ratios. It demonstrated that there were stronger electronic interactions between Zr^{4+}, Ni^{2+} and Fe^{3+} for NiFeZr LDHs with Fe:Zr (1:1).

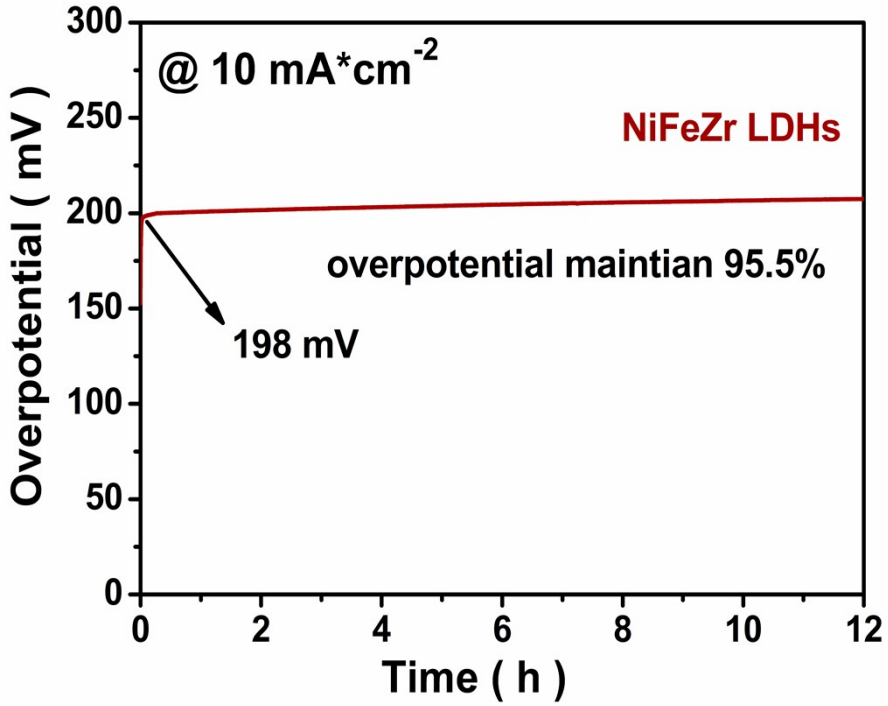

Fig. S6 Potential testing at constant current densities of 10 mA cm^{-2} on the NiFeZr LDHs electrode. The accurate overpotential of NiFeZr LDHs was 198mV to achieve10 mA cm^{-2} according to the galvanostatic measurement without the effect of the nickel anode signal.

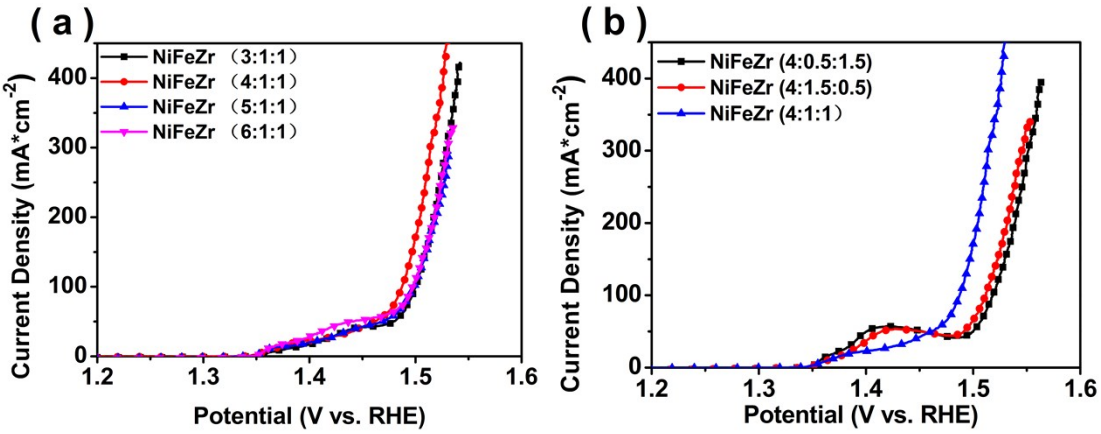

Fig. S7 Polarization curves of the NiFeZr LDHs catalysts with different starting material feed ratio of metal salts.

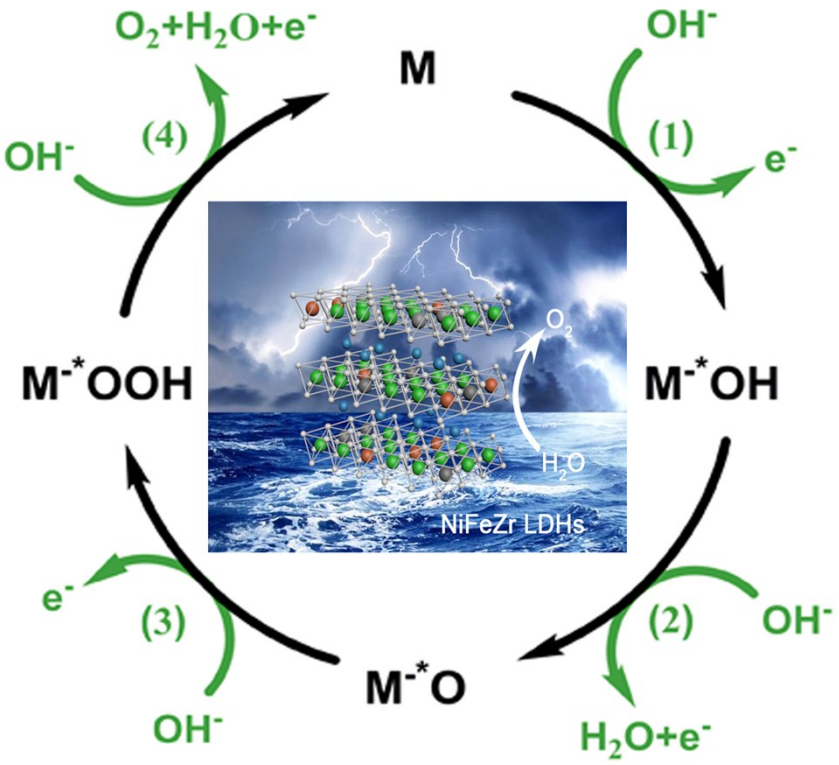

Fig. S8 The OER reaction mechanism in alkaline conditions.

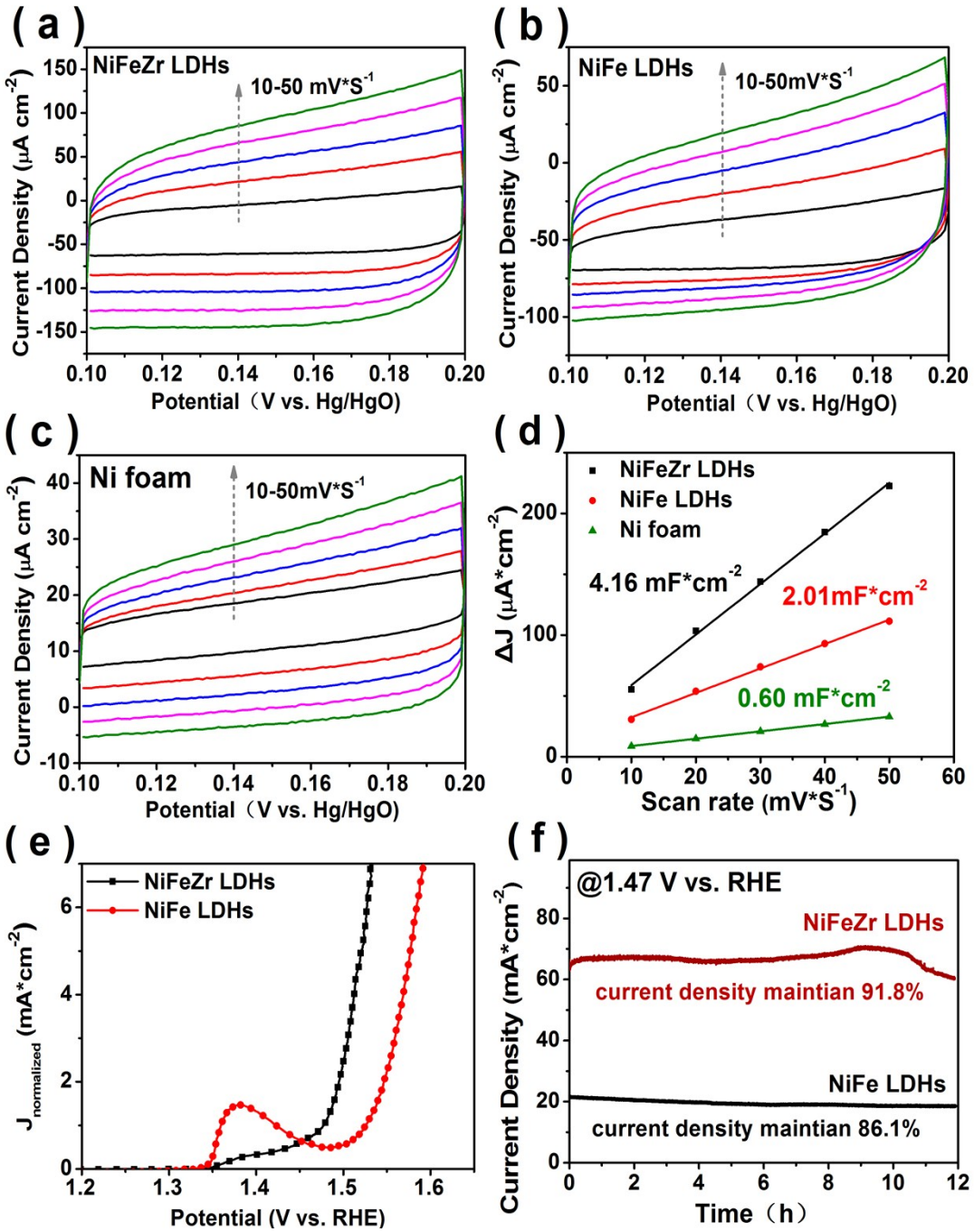

Fig. S9 Electrochemical measurements of the double-layer capacitance of (a) NiFeZr LDHs, (b) NiFe LDHs, (c) Ni foam electrodes at the non-Faradic region (0.1-0.2 V vs. Hg/HgO) with various scan rates (10 mV/s-50mV/s). (d) The normalized LSV curves of NiFeZr LDHs and NiFe LDHs. (e) The Cdl calculations of NiFeZr LDHs, NiFe LDHs, and Ni foam. (f) The potentiostatic stability test of NiFeZr LDHs and NiFe LDHs.

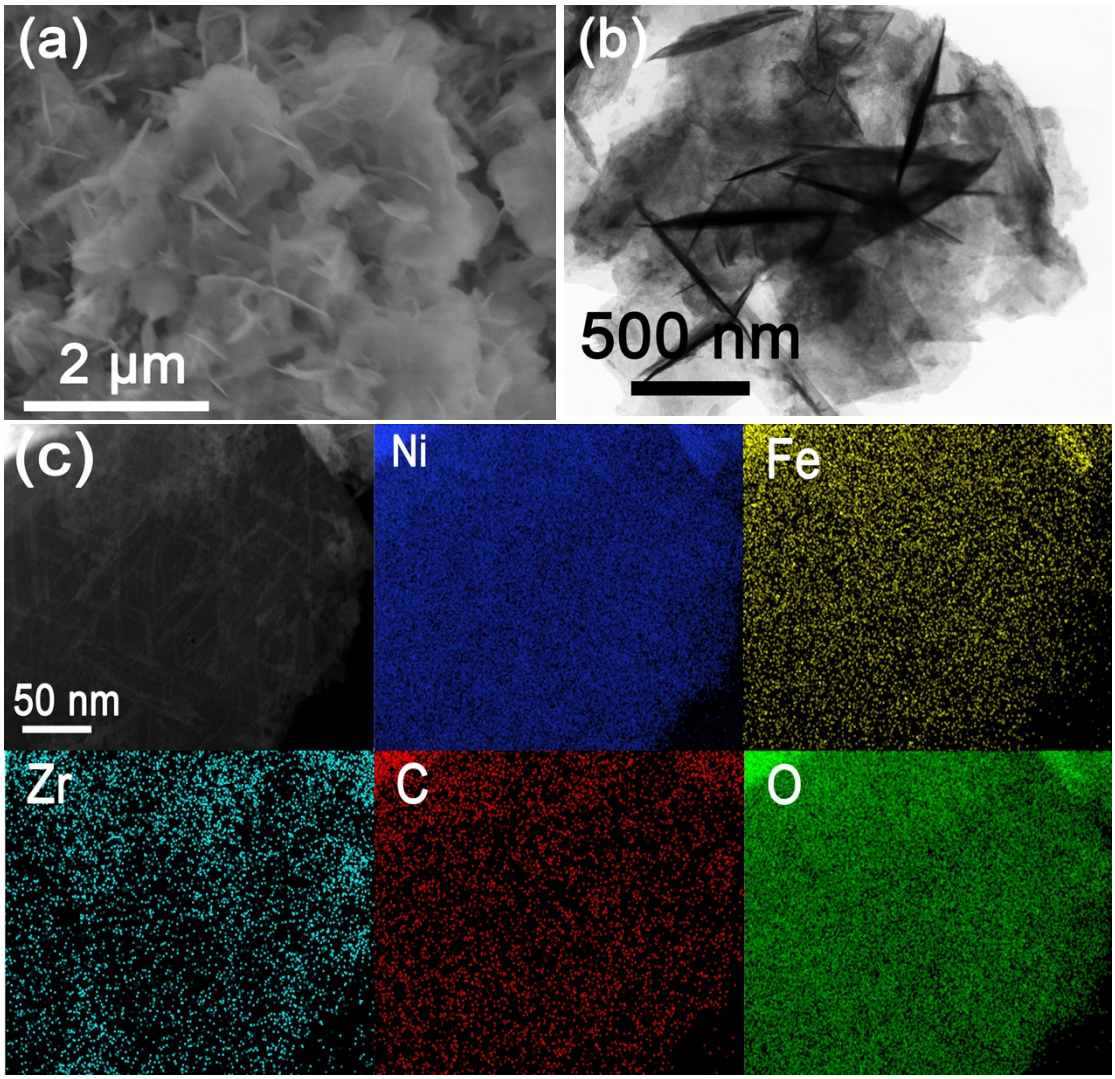

Fig. S10 (a) SEM image, (b) TEM image, (c) HAADF-STEM and elemental mapping images of NiFeZr LDHs nanosheets after the potentiostatic stability test for 12 h.

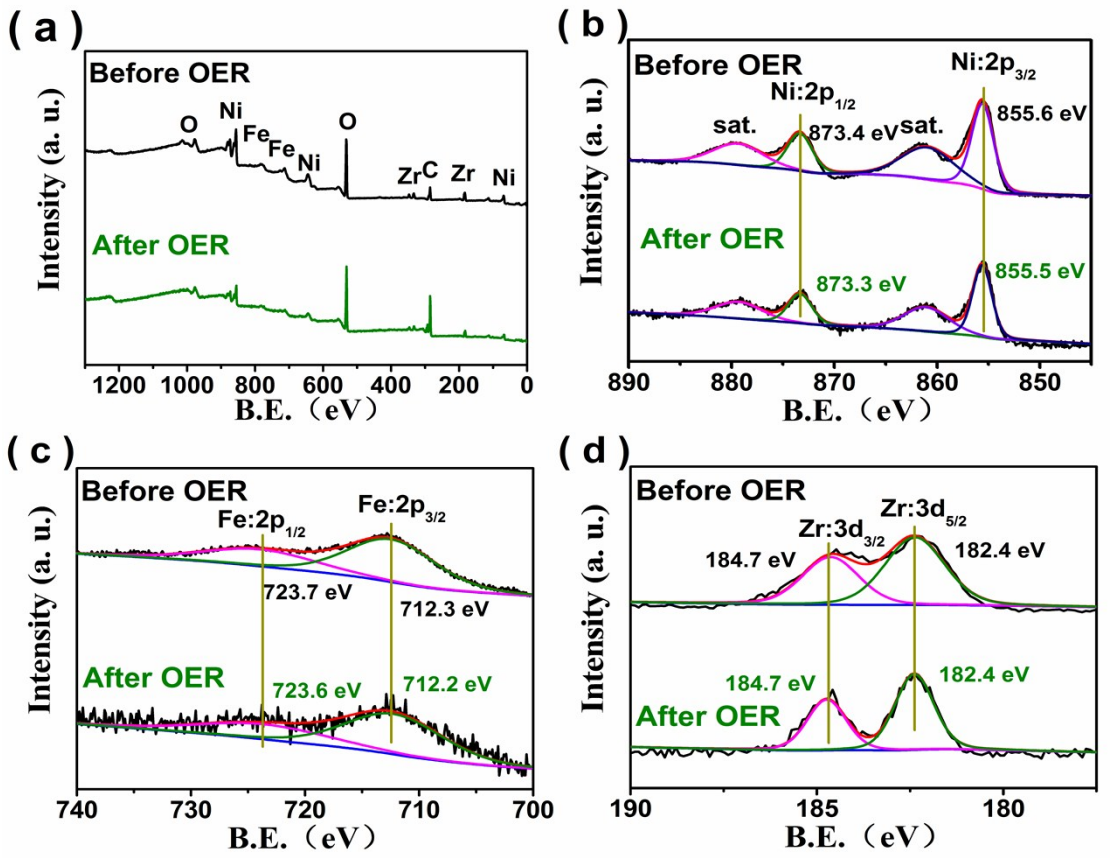

Fig. S11 (a) The XPS profile survey spectra, and High resolution XPS spectrums of (a) Ni 2p, (b) Fe 2p, (c) Zr 3d for NiFeZr LDHs for the NiFeZr LDHs before and after the potentiostatic stability test at 1.47 V vs. RHE for 12 h in1M KOH.

3. Table

Table S1 The percentages of metal atoms on the surface of the catalysts obtianed from XPS.

Catalyst / Atomic %	NiFeZr LDHs (4:1:1)	NiFe LDHs	NiFeZr LDHs (4:0.5:1.5)	NiFeZr LDHs (4:1.5:0.5)
Ni	14.99	12.7	15.11	18.05
Fe	5.55	4.61	4.03	6.22
Zr	2.29	-	3.31	0.69
C	28.71	38.8	34.66	29.69
O	48.45	43.89	42.9	45.35

The surface metal ratio was about 4: 1.5: 0.6 (Ni:Fe:Zr) for NiFeZr LDHs (4:1:1) from the XPS data, different from the EDS result (≈ 4: 1: 1) (Fig. S3b). It indicated the presence of potential surface element separation, which could be related to the electronic interactions between Ni, Fe, and Zr elements.

Table S2 Comparison of OER activities of different NiFe based systems.

Catalyst	Support	Electrolyte	Overpotential (mV)	Tafel slope (mV/dec)	Reference
NiFeZr LDHs	NF	1.0 M KOH	198 (10mA/cm^2)	53.1	This work
^{s}Au/NiFe LDH	TM	1.0 M KOH	237 (10mA/cm^2)	36	1
NiFeV LDHs	NF	1.0 M KOH	195 (20mA/cm^2)	42	2
NiFeCr LDH	CP	1.0 M KOH	280 (10mA/cm^2)	129	3
Fe-doped β-Ni(OH)$_2$	NF	1.0 M KOH	219 (10mA/cm^2)	53	4
Ce-Doped NiFe LDH	CNT	1.0 M KOH	227 (10mA/cm^2)	33	5
S-NiCoFe LDH	CC	1.0 M KOH	206 (10mA/cm^2)	46	6
flame-engraved NiFe-LDH	NF	0.1 M KOH	250 (10mA/cm^2)	69	7
Cu@NiFe LDH	CF	1.0 M KOH	199(10mA/cm2)	27.8	8
(Ni2Co$_1$)$_{0.925}$Fe$_{0.075}$-MOF	GC	1.0 M KOH	257 (10mA/cm^2)	41.3	9
NiFe/Co$_9$S$_8$/CC	CC	1.0 M KOH	219 (10mA/cm^2)	55	10

TM: Ti mesh, NF: Ni foam, GC: glassy carbon, CP: carbon paper, CNT: carbon nanotube, CC: carbon cloth, CF: Cu foam.

Reference

1. J. Zhang, J. Liu, L. Xi, Y. Yu, N. Chen, S. Sun, W. Wang, K. M. Lange and B. Zhang, *J Am. Chem. Soc.*, 2018, **140**, 3876-3879.
2. P. Li, X. Duan, Y. Kuang, Y. Li, G. Zhang, W. Liu and X. Sun, *Adv. Energy Mater.*, 2018, **8**, 1703341.
3. Y. Yang, L. Dang, M. J. Shearer, H. Sheng, W. Li, J. Chen, P. Xiao, Y. Zhang, R. J. Hamers and S. Jin, *Adv. Energy Mater.*, 2018, **8**, 1703189.
4. T. Kou, S. Wang, J. L. Hauser, M. Chen, S. R. J. Oliver, Y. Ye, J. Guo and Y. Li, *ACS Energy Lett.*, 2019, **4**, 622-628.
5. H. Xu, B. Wang, C. Shan, P. Xi, W. Liu and Y. Tang, *ACS Appl. Mater. Interfaces*, 2018, **10**, 6336-6345.
6. L.-M. Cao, J.-W. Wang, D.-C. Zhong and T.-B. Lu, *J. Mater. Chem. A*, 2018, **6**, 3224-3230.
7. D. Zhou, X. Xiong, Z. Cai, N. Han, Y. Jia, Q. Xie, X. Duan, T. Xie, X. Zheng, X. Sun and X. Duan, *Small Methods*, 2018, **2**, 1800083.
8. L. Yu, H. Zhou, J. Sun, F. Qin, F. Yu, J. Bao, Y. Yu, S. Chen and Z. Ren, *Energy Environ. Sci.*, 2017, **10**, 1820-1827.
9. Q. Qian, Y. Li, Y. Liu, L. Yu and G. Zhang, *Adv. Mater.*, 2019, **31**, e1901139.
10. C. Zhan, Z. Liu, Y. Zhou, M. Guo, X. Zhang, J. Tu, L. Ding and Y. Cao, *Nanoscale*, 2019, **11**, 3378-3385.